A Low-Rank and Sparse Matrix Decomposition-Based Mahalanobis Distance Method for Hyperspectral Anomaly Detection

Yuxiang Zhang, *Student Member, IEEE*, Bo Du, *Senior Member, IEEE*, Liangpei Zhang, *Senior Member, IEEE*, and Shugen Wang, *Member, IEEE*

***Abstract*—Anomaly detection is playing an increasingly important role in hyperspectral image (HSI) processing. The traditional anomaly detection methods mainly extract knowledge from the background and use the difference between the anomalies and the background to distinguish them. Anomaly contamination and the inverse covariance matrix problem are the main difficulties with these methods. The low-rank and sparse matrix decomposition (LRaSMD) technique may have the potential to solve the aforementioned hyperspectral anomaly detection problem since it can extract knowledge from both the background and the anomalies. This paper proposes an LRaSMD-based Mahalanobis distance method for hyperspectral anomaly detection (LSMAD). This approach has the following capabilities: 1) takes full advantage of the LRaSMD technique to set the background apart from the anomalies; 2) explores the low-rank prior knowledge of the background to compute the background statistics; and 3) applies the Mahalanobis distance differences to detect the probable anomalies. Extensive experiments were carried out on four HSIs, and it was found that LSMAD shows a better detection performance than the current state-of-the-art hyperspectral anomaly detection methods.**

***Index Terms*—Anomaly detection, hyperspectral imagery, low rank, sparse.**

I. Introduction

HYPERSPECTRAL remote sensing is now a useful and popular type of Earth observation technology for recognizing ground surface materials. Compared with the traditional panchromatic and multispectral remote sensing images, hyperspectral images (HSIs) can provide almost continuous spectral curves of the materials on the ground surface, as the spectral resolution of most hyperspectral spectrometers is less than 10 nm [1]–[4]. With the characteristic of high spectral resolution, hyperspectral remote sensing images with hundreds and even thousands of spectral bands have unique advantages in the field of ground object identification techniques such as target detection and classification [1], [2], [5].

Target detection is essentially a binary classification problem, which aims to separate specific target pixels from various backgrounds [1]. Anomaly detection is an unsupervised target detection technique where no prior knowledge about the target or the background is available, focusing on distinguishing unusual materials from a typical background [1]. Anomalies usually refer to unusual observations or objects with significantly different spectral features from the homogenous background. The background refers to nontarget pixels that are predominant in an image compared with the target pixels [5]. However, it may sometimes be difficult to obtain the prior spectra of the objects of interest. Anomaly detection methods have therefore been the subject of attention in many HSI applications [2]. Moreover, as spectral variability needs to be addressed in supervised target detection [1], the multiplicity of possible spectra associated with the objects of interest has led to the development and application of anomaly detectors. In recent years, hyperspectral anomaly detection has become a booming research topic and has been successfully applied in many application fields, such as mineral reconnaissance, border monitoring, and search and rescue [1], [2], [4], [5].

The current anomaly detection methods mainly extract knowledge from the background and use the difference between the anomaly targets and the background to distinguish them. According to the different ways of extracting knowledge from the background, a great number of anomaly detection methods have been proposed in recent decades. One approach considers the background as a single type and assumes that the entire background obeys a Gaussian normal distribution. The RX detector proposed by Reed and Yu [3] is typical of this type of method, and Schaum [4] later proposed a subspace version, which is called subspace RX (SSRX). The RX and SSRX algorithms are the most widely used methods in hyperspectral anomaly detection. However, these methods use all the pixels in a local region or an entire image scene to compute the background statistics. Thus, the background mean and covariance matrix are susceptible to contamination by anomalies [5],

Manuscript received December 25, 2014; revised April 20, 2015 and July 19, 2015; accepted September 7, 2015. Date of publication October 6, 2015; date of current version February 24, 2016. This work was supported in part by the National Basic Research Program of China (973 Program) under Grant 2011CB707105 and Grant 2012CB719905, by the National Natural Science Foundation of China under Grant 61471274 and Grant 41431175, by the Natural Science Foundation of Hubei Province under Grant 2014CFB193, and by the Fundamental Research Funds for the Central Universities under Grant 2042014kf0239.

Y. Zhang and S. Wang are with the School of Remote Sensing and Information Engineering, Wuhan University, Wuhan 430079, China (e-mail: zyx_070504@163.com; wangsg@whu.edu.cn).

B. Du is with the School of Computer, Wuhan University, Wuhan 430079, China (e-mail: gunspace@163.com).

L. Zhang is with the State Key Laboratory of Information Engineering in Surveying, Mapping and Remote Sensing, Wuhan University, Wuhan 430079, China (e-mail: zlp62@whu.edu.cn).

Color versions of one or more of the figures in this paper are available online at http://ieeexplore.ieee.org.

Digital Object Identifier 10.1109/TGRS.2015.2479299

0196-2892 © 2015 IEEE. Personal use is permitted, but republication/redistribution requires IEEE permission.
See http://www.ieee.org/publications_standards/publications/rights/index.html for more information.

Authorized licensed use limited to: FUDAN UNIVERSITY. Downloaded on February 26,2022 at 02:06:20 UTC from IEEE Xplore. Restrictions apply.

[6], which can weaken the difference between the anomalies and the background. Furthermore, there is also the inverse covariance matrix problem, which usually leads to an unstable approximation, particularly when the inverse covariance matrix is estimated from a local image. Billor *et al.* [7] proposed the blocked adaptive computationally efficient outlier nominator (BACON) anomaly detector, which uses the robust statistics computed from the subsets of the entire hyperspectral data set to suppress the anomaly contamination of the background statistical variables. There are also other detectors capable of alleviating covariance contamination caused by anomalies [8], [9]. One approach estimates an enclosing hypersphere around the background in a high-dimensional feature space and treats pixels that lie outside the hypersphere as outliers. Local support vector data description is a typical method. Although this kind of method can reasonably be adopted in homogeneous areas, the results are often unstable when the local background contains large disturbances or multiple classes [10], [11]. Another kind of approach assumes that the background image is low rank, while anomalies are preserved in the residual image. The robust principal component analysis (RPCA)-based anomaly detector is a typical example, which aims to recover a low-rank matrix from highly corrupted data by the sparse noise [12]. Although these approaches can produce accurate estimation of the background, they cannot easily distinguish between anomalies and noise [13], [14].

Recently, researchers have tried to extract knowledge about both the background and the anomalies from the HSI [15], [16], which may provide more valuable information than those methods exploring only the background information to distinguish anomalies from background. In an HSI, the spectra are usually corrupted with noise caused by the precision limits of the imaging spectrometer, errors in atmospheric variation, etc. The noise can be usually modeled as identically and independently distributed Gaussian random variables [5]. In addition, hyperspectral imagery is usually smooth in the sense that neighboring pixels usually consist of similar materials and have similar spectral characteristics. Due to the strong interband correlations, each spectral vector in the smooth and continuous background in the HSI can be approximately represented as the linear combination of several basis vectors (such as endmembers) [17]. Therefore, the background is usually assumed to lie on a certain low-dimensional subspace, having a low-rank property. On the other hand, the anomalies account for only a small part of the entire image scene; therefore, the anomalies are assumed to be randomly distributed and have a low probability. In other words, they have a sparse property.

Based on the aforementioned analysis, the low-rank and sparse matrix decomposition (LRaSMD) technique [18]–[20], which decomposes a matrix as the sum of a low-rank matrix, a sparse matrix, and a noise matrix, is consistent with the hyperspectral anomaly detection problem. Therefore, with the LRaSMD technique applied to the hyperspectral anomaly detection problem, the valuable signals can be restored and separated from the noise, and the background component can be further separated from the restored signals. In recent years, some researchers have made efforts to employ the LRaSMD technique for hyperspectral anomaly detection. Based on the sparse matrix of the entire image, Cui *et al.* [15] scored each pixel by the norm of the corresponding sparse component vector, and Sun *et al.* [16] scored each pixel with the Euclidean distance between the corresponding sparse component vector and the mean vector of the sparse matrix, which can be labeled as EDLRaSMD. However, these two LRaSMD-based anomaly detectors do not fully consider the internal characteristics of HSIs aforementioned: 1) they pay most attention to the sparse component while ignoring the background component, which has a suppressed anomaly contamination effect since the background component is separated from the sparse component; 2) they utilize the Euclidean distance rather than the Mahalanobis distance, which has proved to be more reasonable for anomaly detection when matched with the HSI Gaussian assumption; and 3) they may make the detection performance worse with more false alarms, since the detection decision relies on the sparse component, which may contain some nonanomaly pixels at larger values of the sparse parameter.

Based on the consistency of the LRaSMD technique and the hyperspectral anomaly detection problem, this paper proposes an LRaSMD-based Mahalanobis distance method for hyperspectral anomaly detection (LSMAD). The proposed method explores both the low-rank prior characteristics of the background and the sparse property of the anomalies to obtain the background and the sparse component. It explores the low-rank prior knowledge of the background to compute the background statistics and constructs a Mahalanobis-distance-based anomaly detector. This way, LSMAD can simultaneously alleviate the anomaly contamination and the inverse covariance matrix problem and improve the detection performance. Although both LSMAD and the RPCA-based anomaly detectors can explore the low-rank and sparse structures from the HSI, they are intrinsically different. The RPCA-based anomaly detectors seek to exactly recover the underlying low-rank background structure and a sparse residual error structure from the original data even in the presence of significant noise. The residual reveals the anomaly energy but is also contaminated by noise, which weakens the detection performance. The LSM detector can alleviate this problem by recovering three structures from the original data: the low-rank background structure, the sparse anomaly structure, and the noise structure. That is to say, the anomaly and the noise are separately modeled in LSMAD.

The rest of this paper is organized as follows. In Section II, the basic RX algorithm and the LRaSMD model are introduced. The proposed LSMAD method is then presented. The experimental results of the proposed method with four HSIs are presented in Section III. Finally, the conclusions are drawn in Section IV.

II. LRaSMD-Based Mahalanobis Distance Method for Anomaly Detection

Anomaly detection aims to distinguish anomaly materials from the background. A good anomaly detector is therefore able to effectively determine the difference between the anomalies and the background and to simultaneously suppress the background. The key process in suppressing the background

Authorized licensed use limited to: FUDAN UNIVERSITY. Downloaded on February 26,2022 at 02:06:20 UTC from IEEE Xplore. Restrictions apply.

is to choose an appropriate method to effectively represent the background. Many anomaly detection algorithms, such as the benchmark RX anomaly detector, use the background covariance matrix to represent the background information.

The RX anomaly detector is conducted based on the hypothesis that the anomaly target and background classes, respectively, follow Gaussian distributions with different mean vectors and the same covariance matrices, where the spectrum of the target and the covariance of the background are unknown. In both the RX anomaly detector and its variants, the inverse of the background covariance matrix is used to measure the statistical difference between the observed test pixel and the background. This procedure can be considered as "spherizing" or "whitening" of the test pixel and the background with elliptical distributions, which produces the corresponding test pixel and background with spherical distributions but with different centers [2]. The RX anomaly detector can be then established as the Euclidean distance between the test pixel and the background in the whitened space, which is actually the Mahalanobis distance in the original space. The RX anomaly detector is specified as

$$D_{\mathrm{RX}}(\mathbf{x}) = (\mathbf{x}-\boldsymbol{\mu})\boldsymbol{\Gamma}^{-1}(\mathbf{x}-\boldsymbol{\mu})^{\mathrm{T}} \tag{1}$$

where $\mathbf{x} = [\mathrm{x}_0\ \mathrm{x}_1, \ldots, \mathrm{x}_B]$ is a B-dimensional hyperspectral pixel vector; and $\boldsymbol{\mu}$ and $\boldsymbol{\Gamma}$ are the mean and the covariance matrix of the input background data, respectively. The background mean and covariance matrix for local detectors can be computed from the processing window. However, the inverse of the background covariance matrix is usually rank deficient and unstable owing to the lack of background training samples for estimation [21]. For simplicity, the statistical variables can be estimated from the whole image. As a result, the anomaly pixels contaminate the background mean and covariance matrix.

The aim of LSMAD is to obtain the representative background from the whole image matrix and to compute an appropriate background covariance matrix while restraining the effect of the anomalies. The background statistics from the obtained background are then computed based on an exploration of the low-rank prior knowledge of the background, which can alleviate the inverse covariance matrix problem.

A. LRaSMD Model for Hyperspectral Imagery

The LRaSMD model was proposed by Zhou *et al.* [22]. It assumes that a low-rank matrix $\mathbf{L} \in \Re^{m\times n}$ from a high-dimensional data matrix is corrupted by gross sparse errors or outliers $\mathbf{S} \in \Re^{m\times n}$. In real-world applications, the observations are often corrupted by noise, which may be stochastic or deterministic. Thus, the observed data $\mathbf{D} \in \Re^{m\times n}$ can be modeled as

$$\mathbf{D} = \mathbf{L} + \mathbf{S} + \mathbf{N} \tag{2}$$

where $\mathbf{N}$ is the noise term, which is usually assumed to be independent and identically distributed Gaussian noise.

The original HSI data cube with the spatial and spectral dimensions of $H \times W \times B$ can be rearranged as a 2-D matrix with the size $N \times B$, in which B represents the number of spectral bands; H and W are the height and width of the image scene, respectively; and N stands for the total number of pixels in the whole image scene. As we know, an image scene is usually continuous and smooth in the sense that neighboring pixels usually consist of similar materials and have similar spectral characteristics. The spectral signatures of the materials in HSI data are highly correlated, and each spectral vector can be therefore approximately represented as the linear combination of several basis vectors. The background image is usually assumed to have a low-rank property. On the other hand, due to the low spatial resolution of the HSI, the anomalies of interest in the HSI data usually have a low probability and account for only a very small part of the entire image scene, which indicates the sparse property of the anomalies.

Based on the aforementioned analysis, the LRaSMD technique is consistent with the hyperspectral anomaly detection problem. Therefore, the model of the HSI can be written as

$$\mathbf{X} = \mathbf{B} + \mathbf{S} + \mathbf{N} \tag{3}$$

where $\mathbf{X} \in \Re^{N\times B}$ is the observed HSI, $\mathbf{B}$ indicates the background image, $\mathbf{S}$ denotes the sparse component, and $\mathbf{N}$ stands for the noise. Clearly, the matrix $\mathbf{B}$ is low rank, and the matrix $\mathbf{S}$ is sparse. It is then natural to employ LRaSMD theory for the observed matrix $\mathbf{X}$ to obtain the background component $\mathbf{B}$ and the sparse component $\mathbf{S}$.

B. Recovery of the Model Components

In recent years, a number of LRaSMD optimization algorithms have been proposed, which concentrate on developing fast approximations and meaningful decompositions [23]. For example, Halko *et al.* [24] proposed representative randomized approximate matrix decomposition (RAMD), which reveals that a matrix can be effectively approximated by its projection onto the column space of its random projections and can be regarded as a fast approximation of singular value decomposition (SVD)/principal component analysis (PCA). Candès *et al.* [12] proposed RPCA, which can provide a blind decomposition of low-rank data and sparse noise.

In this paper, we adopt the GoDec algorithm proposed by Zhou and Tao [25] to solve the low-rank background component and the sparse component. GoDec is a fast approximation algorithm, which replaces the time-consuming SVD/PCA with the bilateral random projections (BRPs) [26] in RAMD. Furthermore, the GoDec algorithm can explore the low-rank and sparse structures and can simultaneously consider the additive noise, which is considered together with the sparse structure in the RPCA decomposition. The BRP-based GoDec problem can be solved by minimizing the decomposition error with the rank and sparse constraints, as follows:

$$\min_{\mathrm{B,S}} \|\mathbf{X}-\mathbf{B}-\mathbf{S}\|_F^2 \quad \text{s.t. } \mathrm{rank}(\mathbf{B}) \le r, \mathrm{card}(\mathbf{S}) \le kN \tag{4}$$

where r and k stand for the upper bound of the rank of $\mathbf{B}$ and the cardinality of $\mathbf{S}$, respectively. The cardinality k of $\mathbf{S}$ reflects the sparse energy in the image scene, which is usually defined as the ℓ_0-norm of $\mathbf{S}$. The background can be approximately

Authorized licensed use limited to: FUDAN UNIVERSITY. Downloaded on February 26,2022 at 02:06:20 UTC from IEEE Xplore. Restrictions apply.

represented as the linear combination of several basis vectors, and the number of the basis vectors is regarded as the rank of the background component matrix. These basis vectors are usually depicted by the background endmembers, background covariance eigenvectors, or other features. The sparse component may contain some background energy; thus, not all the background materials are taken into consideration when determining the rank value of the low-rank component. Therefore, the value of r can be set according to the number of dominant background endmembers or background classes. The detailed parameter analysis will be further investigated in the following experimental section.

The optimization problem in (4) can be converted into alternately solving the following two subproblems until convergence:

$$\mathbf{B}_t = \arg \min_{\text{rank}(\mathbf{B})\le r} \|\mathbf{X}-\mathbf{B}-\mathbf{S}_{t-1}\|_F^2 \tag{5}$$

$$\mathbf{S}_t = \arg \min_{\text{card}(\mathbf{S})\le kN} \|\mathbf{X}-\mathbf{B}_{t-1}-\mathbf{S}\|_F^2. \tag{6}$$

BRP-based low-rank approximation theory is employed to solve the subproblem in (5). Suppose that

$$\mathbf{Y}_1 = \mathbf{X}\mathbf{A}_1 \quad \mathbf{Y}_2 = \mathbf{X}^T\mathbf{A}_2 \tag{7}$$

where $\mathbf{A}_1 \in \Re^{B\times r}$ and $\mathbf{A}_2 \in \Re^{N\times r}$ are random matrices. For simplicity, $\mathbf{A}_1$ can be obtained using the MATLAB randn function, which can generate a random matrix following a standard normal distribution, and $\mathbf{A}_2$ can be obtained by $\mathbf{A}_2 = \mathbf{Y}_1 = \mathbf{X}\mathbf{A}_1$.

The BRP-based rank-r approximation of $\mathbf{X} \in \Re^{N\times B}$ is

$$\mathbf{B} = \mathbf{Y}_1\left(\mathbf{A}_2^T\mathbf{Y}_1\right)^{-1}\mathbf{Y}_2^T. \tag{8}$$

As for the subproblem in (6), $\mathbf{S}_t$ is updated via entrywise hard thresholding of $\mathbf{X}-\mathbf{B}_{t-1}$, i.e.,

$$\mathbf{S}_t = P_\Omega(\mathbf{X}-\mathbf{B}_{t-1}), \quad \Omega : \left|(\mathbf{X}-\mathbf{B}_{t-1})_{i,j\in\Omega}\right| \ne 0 \text{ and } \ge \left|(\mathbf{X}-\mathbf{B}_{t-1})_{i,j\in\bar{\Omega}}\right|, \quad |\Omega| \le kN \tag{9}$$

where $P_\Omega(\cdot)$ is the projection of a matrix onto an entry set Ω, and Ω is the nonzero subset of the first kN largest entries of $|\mathbf{X}-\mathbf{B}_{t-1}|$.

The GoDec algorithm can be summarized as Algorithm 1.

C. Mahalanobis-Distance-Based Anomaly Detection

After the recovery of both the low-rank background matrix and the sparse matrix, the low-rank background matrix captures the global background information, the sparse matrix contains the anomaly information, and the background and the anomalies are separated. Thus, the statistical features of the background can be obtained from the background matrix. We can then use the statistical features to build a Mahalanobis-distance-based anomaly detector. The detector is assumed to suppress the anomaly contamination problem. The detector can be represented as follows:

$$D_{\text{LSMAD}}(\mathbf{x}) = (\mathbf{x}-\boldsymbol{\mu}_b)^{\mathrm{T}}\boldsymbol{\Gamma}_b^{-1}(\mathbf{x}-\boldsymbol{\mu}_b) \tag{10}$$

where $\boldsymbol{\mu}_b$ and $\boldsymbol{\Gamma}_b$ are the mean and the covariance matrix of the input background data, respectively, which can be estimated from the recovered background component $\mathbf{B} = [\mathbf{B}_1, \ldots, \mathbf{B}_N]$, as follows:

$$\boldsymbol{\mu}_b = \frac{1}{N}(\mathbf{B}_1 + \cdots + \mathbf{B}_N) \tag{11}$$

$$\boldsymbol{\Gamma}_b = \frac{1}{N}(\mathbf{B}-\boldsymbol{\mu}_b)^{\mathrm{T}} \times (\mathbf{B}-\boldsymbol{\mu}_b). \tag{12}$$

The eigendecomposition of the background covariance matrix $\boldsymbol{\Gamma}_b$ is

$$\boldsymbol{\Gamma}_b = \mathbf{V}\mathbf{A}\mathbf{V}^T \tag{13}$$

where $\mathbf{V} = [\mathbf{V}_1\ \mathbf{V}_2, \ldots, \mathbf{V}_B]$ is the eigenvector matrix, $\mathbf{A} = \text{diag}(\lambda_1\ \lambda_2, \ldots, \lambda_B)$ is the eigenvalue matrix, and $\lambda_1 \ge \lambda_2 \ge \cdots \ge \lambda_B$. The inverse covariance matrix can be given by

$$\boldsymbol{\Gamma}_b{}^{-1} = \mathbf{V}\mathbf{A}^{-1}\mathbf{V}^T = \sum_{i=1}^{B} \lambda_i{}^{-1}\mathbf{V}_i\mathbf{V}_i^T. \tag{14}$$

Algorithm 1: Godec algorithm

Input: a) $\mathbf{X} \in \Re^{N\times B}$, the data matrix
a) r, the maximal rank of the background matrix
b) k, the cardinality of the sparse matrix
c) ε, the error tolerance
d) $Iter$, the maximum iteration number
Output: $\mathbf{B}$, the low-rank matrix approximation
$\mathbf{S}$, the sparse matrix approximation

Step (1): Initialize: $\mathbf{B}_0 = \mathbf{X}, \mathbf{S}_0 := 0, t := 0, \mathbf{A}_1 = \text{randn}(B, r)$
Step (2): Repeat $Iter$ times
a) $t := t+1$
b) $\mathbf{Y}_1 = (\mathbf{X}-\mathbf{S}_{t-1})\mathbf{A}_1, \quad \mathbf{A}_2 = \mathbf{Y}_1, \quad \mathbf{Y}_2 = (\mathbf{X}-\mathbf{S}_{t-1})^T\mathbf{A}_2$
c) If $\text{rank}(\mathbf{A}_2^T\mathbf{Y}_1) < r$ then $r := \text{rank}(\mathbf{A}_2^T\mathbf{Y}_1)$, go to step b); end;
d) $\mathbf{B}_t = \mathbf{Y}_1(\mathbf{A}_2^T\mathbf{Y}_1)^{-1}\mathbf{Y}_2^T$
e) $\mathbf{S}_t = P_\Omega(\mathbf{X}-\mathbf{B}_{t-1})$
Until $\|\mathbf{X}-\mathbf{B}_t-\mathbf{S}_t\|_F^2/\|\mathbf{X}\|_F^2 < \varepsilon$

The inverse of the background covariance matrix is usually rank deficient due to the deficient training samples, particularly in the local methods, and it will be unstable when there is one certain eigenvalue λ_i that is too small and makes λ_i^{-1} clearly increase. Due to the low-rank property of the background component, the background component can be represented as the linear combination of several basis vectors, and the number of the basis vectors is equal to the rank of the background component matrix. These basis vectors are usually depicted by the eigenvectors of the background covariance matrix. The low-rank background can be therefore represented by several eigenvectors of the background covariance matrix, and the value of the selected eigenvectors depends on the rank value. The inverse background covariance matrix can be then estimated

Authorized licensed use limited to: FUDAN UNIVERSITY. Downloaded on February 26,2022 at 02:06:20 UTC from IEEE Xplore. Restrictions apply.

by the first r largest eigenvalues and their corresponding eigenvectors, as follows:

$$\mathbf{\Gamma}_b{}^{-1} = \sum_{i=1}^{r} \lambda_i{}^{-1} \mathbf{V}_i \mathbf{V}_i{}^{\mathrm{T}}. \tag{15}$$

LSMAD is a Mahalanobis-distance-based anomaly detector that fully utilizes the background component and its prior low-rank knowledge. Research in the past decade has proved the ability of the Mahalanobis distance to detect anomalies from complex backgrounds [27]–[29]. The key assumption of these Mahalanobis-distance-based methods is that the statistical features of the anomalies and the background can be depicted by the mean and covariance matrix. Hence, the main difference between these methods is the different ways of computing the mean and covariance matrix of the background. For the original RX and SSRX, they make the background estimation without the anomaly-free assumption. Meanwhile, BACON uses an initial subset assumed to be free of anomalies, and this has a considerable effect on the final background pixel set. The proposed LSMAD does not find an optimal initial subset, but defines the number of nonzero pixels in the sparse matrix. The LRaSMD process is then performed a sufficient number of times to ensure that the decomposition error is minimized with the low-rank and sparse constraints, which can restore the signal from the noise and further separate the background from the sparse materials, including the anomalies. In addition, although the sparse pixels may not be the optimal anomalies of interest, and they may include other sparse background materials, this will not have a noticeable effect on the majority of the background statistical variables. In addition to the alleviation of the anomaly contamination issue, the LSMAD method further explores the low-rank prior knowledge of the background component for the inverse covariance matrix estimation, which can avoid the singular and unstable inverse covariance matrix problem in the local Mahalanobis-distance-based detectors.

LSMAD provides a new perspective to LRaSMD for hyperspectral anomaly detection and concentrates on the reliable background component. In the previous studies [15], [16], the sparse component among the three components in (3) has been the preference for the anomaly detection, and the norm or the Euclidean distance of the sparse component has been utilized to develop the anomaly detectors. The key assumption of these sparse-component-based detectors is that the sparse component conveys the information about the anomalies of interest, and the detection statistic of each pixel relies only on the corresponding sparse component vector, which ignores the background component and the original image information of the pixel. However, the background-component-based LSMAD is more robust than the sparse-component-based detectors. In detail, the anomaly energy is usually not effectively extracted during the LRaSMD recovery process. As shown in Fig. 1, the anomaly energy is reflected not only by the sparse matrix S but also by the background matrix, and even by the noise matrix, which will influence the detection probability of the sparse-component-based detectors. Furthermore, as shown in Fig. 2, the sparse component usually contains both anomalies and sparse background materials, which may ultimately increase the false alarms. However, even if there is still anomaly contamination of the background component during the LRaSMD recovery process, the effect of the anomaly contamination on LSMAD can be finally suppressed. The reason for this is that the eigenvectors with lower eigenvalues containing much anomaly information are rejected for the inverse covariance matrix estimation.

(a) (b) (c)

Fig. 1. Recovery performance when the anomaly energy is insufficiently extracted at $k = 0.1$ in the PaviaC data set.

(a) (b) (c)

Fig. 2. Recovery performance when the background component and the sparse component are not well separated at $k = 0.5$ in the PaviaC data set.

III. Hyperspectral Data Experiments

A. Hyperspectral Data Sets and Experimental Platform

Four hyperspectral data sets were used in this study to evaluate the effectiveness of the proposed detector introduced in Section II. We used four data sets with different characteristics, including the data collection instrument, the target size, and the spatial distribution of the targets. The experimental platform was a personal computer with an Intel(R) Core(TM) i3 2.20-GHz central processing unit, 4-GB memory, and 64-bit Windows 7. All the algorithms were implemented in MATLAB 2014a.

The first data set was collected by the Reflective Optics System Imaging Spectrometer sensor [16]. It is a scene of Pavia city center in northern Italy, as shown in Fig. 3(a). The image scene covers an area of 108 × 120 pixels, with 102 spectral bands in wavelengths ranging from 430 to 860 nm, with a 1.3-m spatial resolution. The main background materials are bridge and water. There are some vehicles on the bridge and bare soil near the bridge pier, which, in total, consist of 43 pixels and account for 0.33% of the image scene, as shown in Fig. 3(b). The spectral signatures of these pixels are different from the main background, as shown in Fig. 3(c), and these pixels were therefore selected as the anomalies to be detected.

The second data set was collected by the Airborne Visible/Infrared Imaging Spectrometer (AVIRIS) from San Diego, CA, USA. The spatial resolution is 3.5 m per pixel [30], [31]. The

Authorized licensed use limited to: FUDAN UNIVERSITY. Downloaded on February 26,2022 at 02:06:20 UTC from IEEE Xplore. Restrictions apply.

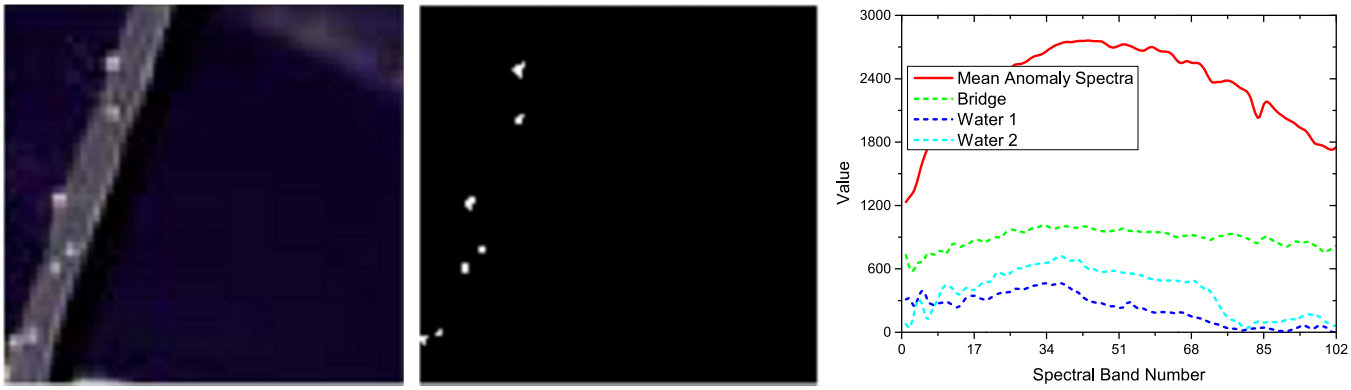

(a) (b) (c)

Fig. 3. (a) PaviaC image scene. (b) Anomaly location. (c) Spectral signatures of the anomaly and background classes.

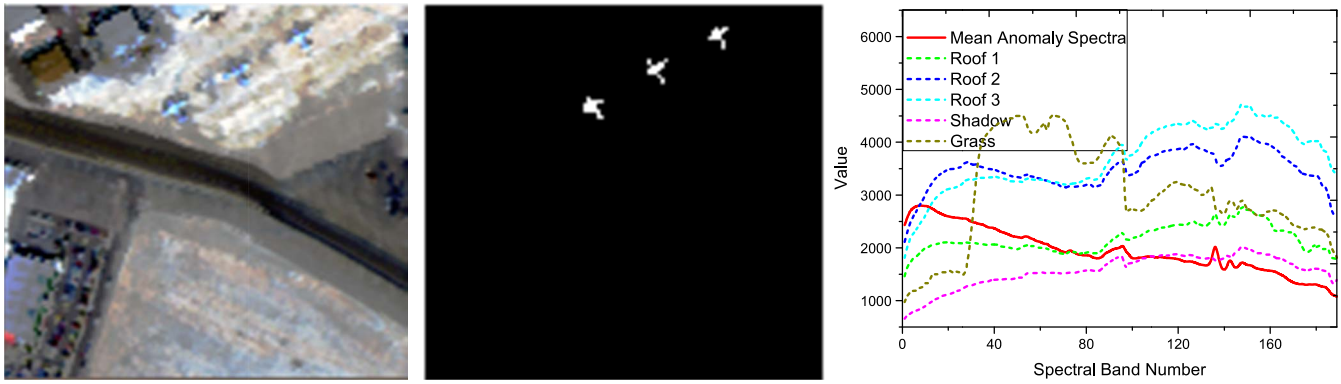

(a) (b) (c)

Fig. 4. (a) AVIRIS image scene. (b) Anomaly location. (c) Spectral signatures of the anomaly and background classes.

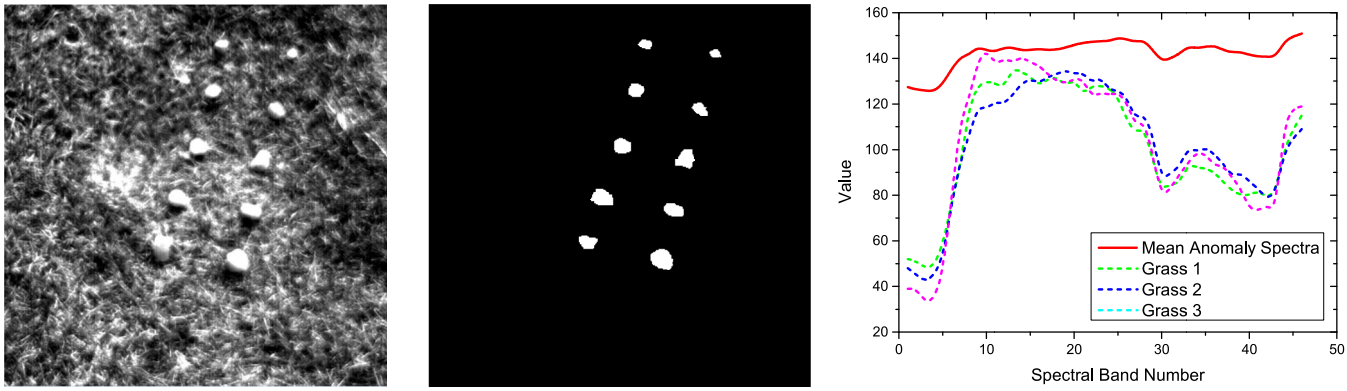

(a) (b) (c)

Fig. 5. (a) Cri image scene. (b) Anomaly location. (c) Spectral signatures of the anomaly and background classes.

image has 224 spectral channels in wavelengths ranging from 370 to 2510 nm. After removing the bands that correspond to the water absorption regions, low signal-to-noise ratio, and bad bands (1–6, 33–35, 97, 107–113, 153–166, and 221–224), 189 available bands of the data were retained in the experiments. From this hyperspectral data set, a region with the size of 120 × 120 pixels was selected to test the detection performance, as shown in Fig. 4(a). This data set is an urban scene in which the main background materials are roof, shadow, and grass. There are three planes in the image, which consist of 58 pixels and account for 0.33% of the image, as shown in Fig. 4(b). The spectral signatures of these planes are different from those of the main background, as shown in Fig. 4(c), and these pixels were therefore selected as the anomalies to be detected.

The third data set was acquired by the Nuance Cri hyperspectral sensor [32]. This sensor can acquire imagery with a spectral resolution of 10 nm. The image scene covers an area of 400 × 400 pixels, as shown in Fig. 5(a), with 46 spectral bands

Authorized licensed use limited to: FUDAN UNIVERSITY. Downloaded on February 26,2022 at 02:06:20 UTC from IEEE Xplore. Restrictions apply.

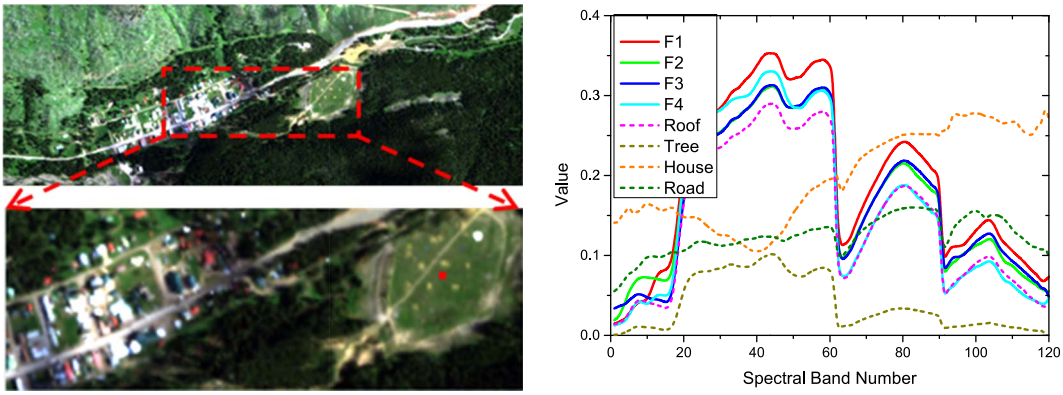

(a) (b)

Fig. 6. (a) HyMap image scene and target F1 location (the red pixels in the right of the subimage). (b) Spectral signatures of the background classes and the four fabric targets.

in wavelengths ranging from 650 to 1100 nm. There are ten rocks located in the grassy scene, which consist of 2216 pixels and account for 1.385% of the image, as shown in Fig. 5(b). The spectral signatures of these rocks are quite different from the main background, as shown in Fig. 5(c), and these pixels were therefore selected as the anomalies to be detected.

The fourth data set is a HyMap image, which was captured at the location of the small town of Cook City, MT, USA, on July 4, 2006 [33], [34]. The image scene covers an area of 200 $\times$ 800 pixels, with 126 spectral bands in wavelengths ranging from 450 to 2500 nm. After removing the bad bands, 120 bands of the data were retained. There are seven types of target in the image, including four fabric panel targets and three vehicle targets. In this experiment, we cropped a residential area subimage of size 100 $\times$ 300, as depicted in Fig. 6(a). The main background types of the subimage are roof, road, grass, and tree; and the spectral signatures of both the background and fabric targets are shown in Fig. 6(b). This data set is challenging for anomaly detection because of the high spectral similarity of the four fabric targets and the background grass class. Target F1 among the four targets has the most different spectral signature compared with the main background, and we therefore regarded it as the anomaly to be detected.

B. Detection Performance and Parameter Analysis

The detection performance and the time consumption of the proposed LSMAD were evaluated and compared with four other state-of-the-art detectors: Global RX (GRX), BACON, SSRX, and EDLRaSMD. The rank value for LSMAD can be set by an empirical method. From the results of the existed publications [16], [35]–[38], we can find that the rank value is usually very small. For example, [16] tested the rank values 2–10, [36] tested the rank values 1–40 and found that the appropriate rank value is small (for example, $r \leq 5$), and [37] set the value as 1. Moreover, based on the analysis of [35], the rank in the LRaSMD model is highly correlated with the number of the main background image classes. We can therefore follow the way of most related publications to determine the rank empirically before the detection procedure and empirically choose a rough rank value for our work. An empirical rank value of 1 or 2 is used for LSMAD. For the data sets with one dominate category, such as PaviaC and HyMap, 1 is set as the rank value. For the data sets with two dominate categories, such as Cri and AVIRIS, 2 is set as the rank value. On the other hand, many existed algorithms can also provide a candidate rank value in this experiment via a respective automatic method, such as the famous hyperspectral signal subspace identification by minimum error (HySime) algorithm [39]. We therefore compare the detection performance with the HySime algorithm or the empirically determined method. The number of components to reject for SSRX can be theoretically chosen based on the eigenvalue investigation. As we know, the larger of the eigenvalues of the covariance matrix are usually several orders of magnitude greater than the smallest in hyperspectral data sets of natural backgrounds [4]. The number of the larger eigenvalues is usually small and close to the number of background materials in the image. Therefore, for convenience, we usually choose the number of components to reject for SSRX according to the number of background classes, which can be also empirically determined or determined via HySime algorithm. The cardinality k of the sparse matrix is set according to the ratio of the anomalies in the image scene (RAI). The experimental results for all the detectors are provided through receiver operating characteristic (ROC) curves for the first three data sets, as shown in Fig. 7(a)–(c). As the number of anomalies in the HyMap data set is small, we provide the experimental results via the false alarm rate (FAR) when the probability of detection reaches 100%, as shown in Fig. 7(d).

For the PaviaC data set, as shown in Fig. 7(a), the result of LSMAD demonstrates a better performance than the other detection algorithms. LSMAD also generates a much better detection performance than EDLRaSMD. LSMAD and EDLRaSMD have FARs of approximately 0.001 and 0.1, respectively, when achieving a 100% probability of detection. The detection performances of BACON and SSRX show an obvious improvement over that of GRX. For the AVIRIS data set, as shown in Fig. 7(b), the ROC curve of LSMAD is always above those of SSRX, BACON, and GRX. Furthermore, the ROC curve of LSMAD is above that of EDLRaSMD when the FAR is less than 0.016. For the Cri data set, as shown in Fig. 7(c), the ROC curves of LSMAD, SSRX, and EDLRaSMD are not separated

Authorized licensed use limited to: FUDAN UNIVERSITY. Downloaded on February 26,2022 at 02:06:20 UTC from IEEE Xplore. Restrictions apply.

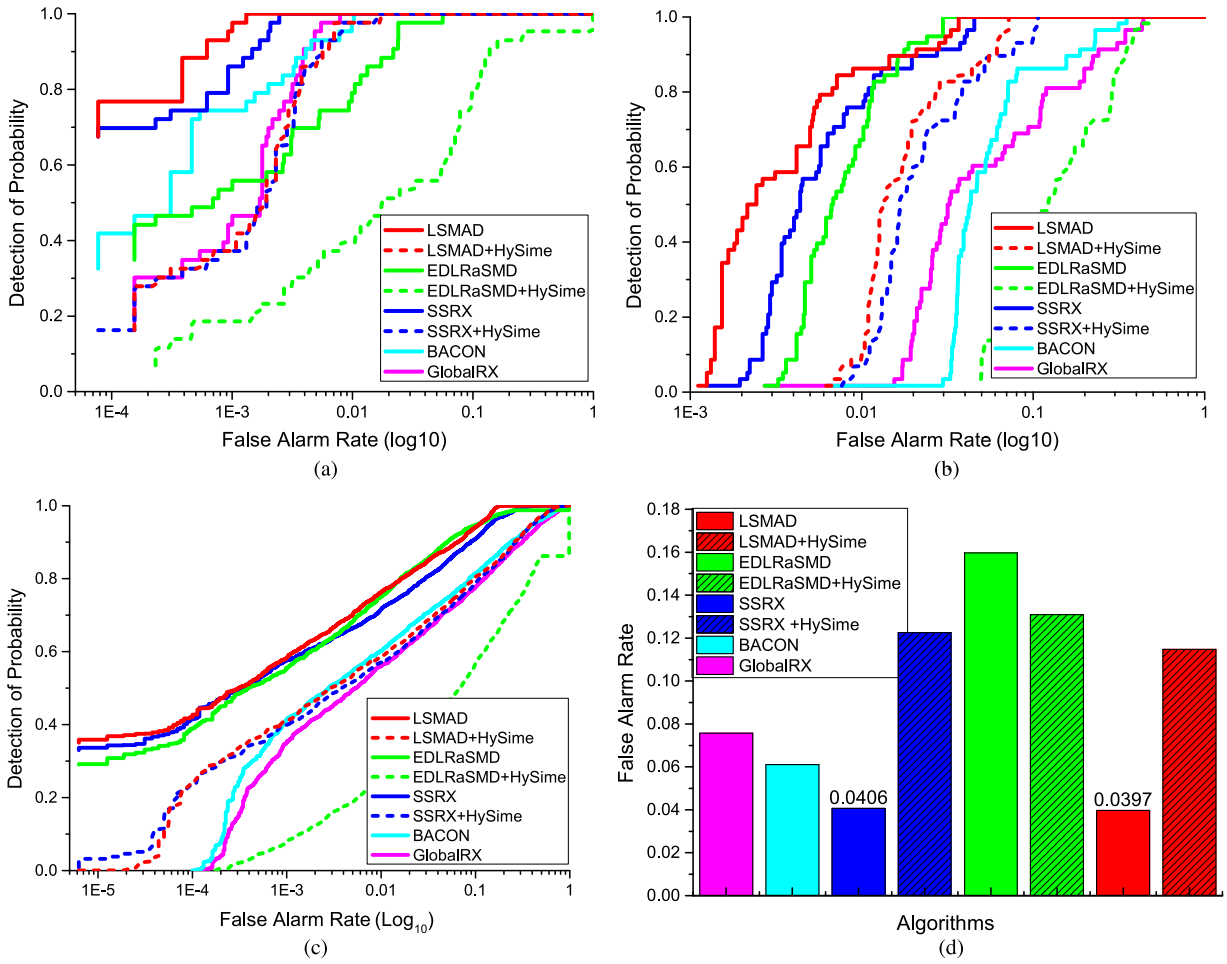

Fig. 7. Detection performance for the four data sets.

TABLE I
TIME CONSUMPTION WITH THE FOUR DATA SETS

Time (s)	GRX	SSRX	BACON	EDLRaSMD	LSMAD
PaviaC	0.14	0.45	24.61	11.40	10.77
AVIRIS	0.33	1.86	42.00	25.20	27.24
Cri	1.50	2.53	885.46	61.73	64.18
HyMap	0.43	2.37	316.22	31.13	29.68

so far as they do in the PaviaC and AVIRIS data sets. Still, the ROC curve of LSMAD is almost always above those of SSRX, BACON, and GRX. In addition, the ROC curve of LSMAD is above that of EDLRaSMD when the FAR is less than 0.0147. For the HyMap data set, the result indicates that the proposed LSMAD provides a better detection performance than the other algorithms. Furthermore, as shown in Table I, the time cost of the proposed LSMAD is acceptable and is approximately the same as that of EDLRaSMD and less than that of BACON.

In general, with the HySime algorithm, the performances of LSMAD, EDLRaSMD, and SSRX, respectively, are decreased compared with those with the empirically determined rank values. With the HySime algorithm, the performance of LSMAD for the PaviaC and HyMap data sets is weaker than GlobalRX and BACON; with the HySime algorithm, LSMAD for the AVIRIS data set still outperforms the other competing algorithms, and the detection performance of LSMAD for the Cri data set is more or less very similar across the GRX, BACON, and SSRX algorithms. Although the existed algorithms, such as the HySime algorithm, can provide a rank candidate without other supplementary information, they may not always provide the satisfactory detection performance.

Overall, with the empirically determined rank values, LSMAD generally performs the best with all four data sets. The main reasons for this superior performance in detection are as follows: 1) because of the essential attribute of the discriminative Mahalanobis-distance-based method, the proposed algorithm learns a hyperplane that can separate the anomalies and background by the Mahalanobis distance; 2) the introduced LRaSMD helps to obtain an effective background estimation for the background and to further grasp the low-rank property for the inverse background covariance matrix estimation; and 3) smaller rank value may be suitable for our data sets since the anomaly samples present an obvious separation with background samples and very few basis vectors can composite the subspace for separating anomalies from backgrounds.

To further analyze the influence of the rank parameter r on the final detection performance of LSMAD, the performance of LSMAD with respect to the rank parameter r of the background matrix was investigated based on the PaviaC, AVIRIS, and Cri data sets. Without loss of generality, we test a large range of r for the three data sets. The cardinality k of the sparse matrix

Authorized licensed use limited to: FUDAN UNIVERSITY. Downloaded on February 26,2022 at 02:06:20 UTC from IEEE Xplore. Restrictions apply.

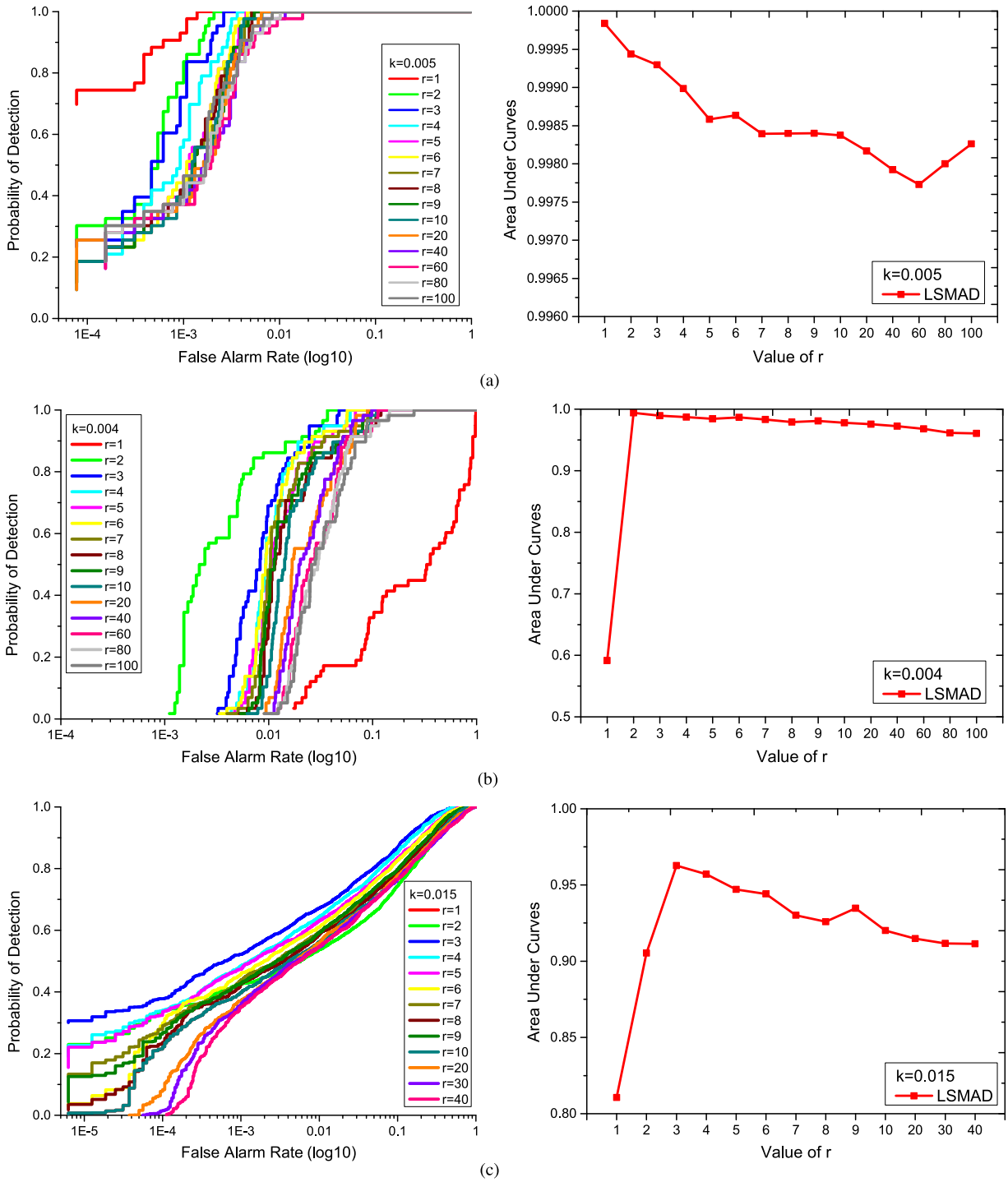

Fig. 8. ROC and AUC performance of LSMAD with respect to the background rank for the three data sets. (a) PaviaC. (b) AVIRIS. (c) Cri.

is related to the RAI. As there are always some false alarms when all the anomalies are detected, we therefore relaxed the RAI value to 0.005, 0.004, and 0.015 as the value of k for the PaviaC, AVIRIS, and Cri data sets, respectively. The experimental results are provided via the ROC curve and the area under curve (AUC), as shown in Fig. 8.

The results in Fig. 8 generally show that the proposed LSMAD presents the best performance with a very low rank value, and then, the detection performance gradually slowly decreases. For the PaviaC data set in Fig. 8(a), LSMAD performs the best when the rank r is equal to 1, and the detection performance gradually and slowly decreases as r increases. For the AVIRIS data set in Fig. 8(b), the detection performance of LSMAD improves as the rank r increases to 2. After that, the detection performance gradually and slowly decreases as r increases. For the Cri data set in Fig. 8(c), the detection performance of LSMAD improves as the rank r increases to 3. After that, the detection performance gradually and slowly decreases as r increases. It is concluded that a very low empirically determined rank value is effective in LSMAD for various HSIs. Most

Authorized licensed use limited to: FUDAN UNIVERSITY. Downloaded on February 26,2022 at 02:06:20 UTC from IEEE Xplore. Restrictions apply.

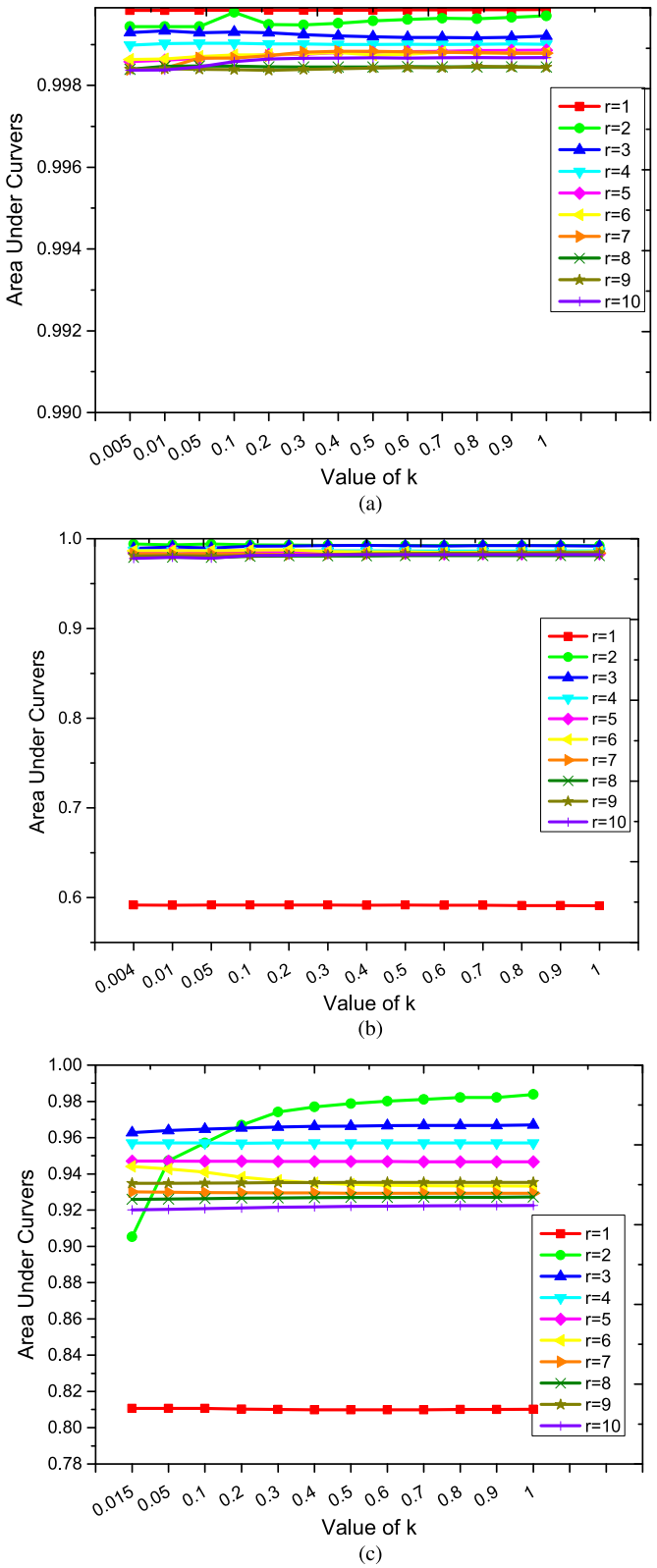

Fig. 9. Performance of LSMAD with respect to the cardinality parameter. (a) PaviaC. (b) AVIRIS. (c) Cri.

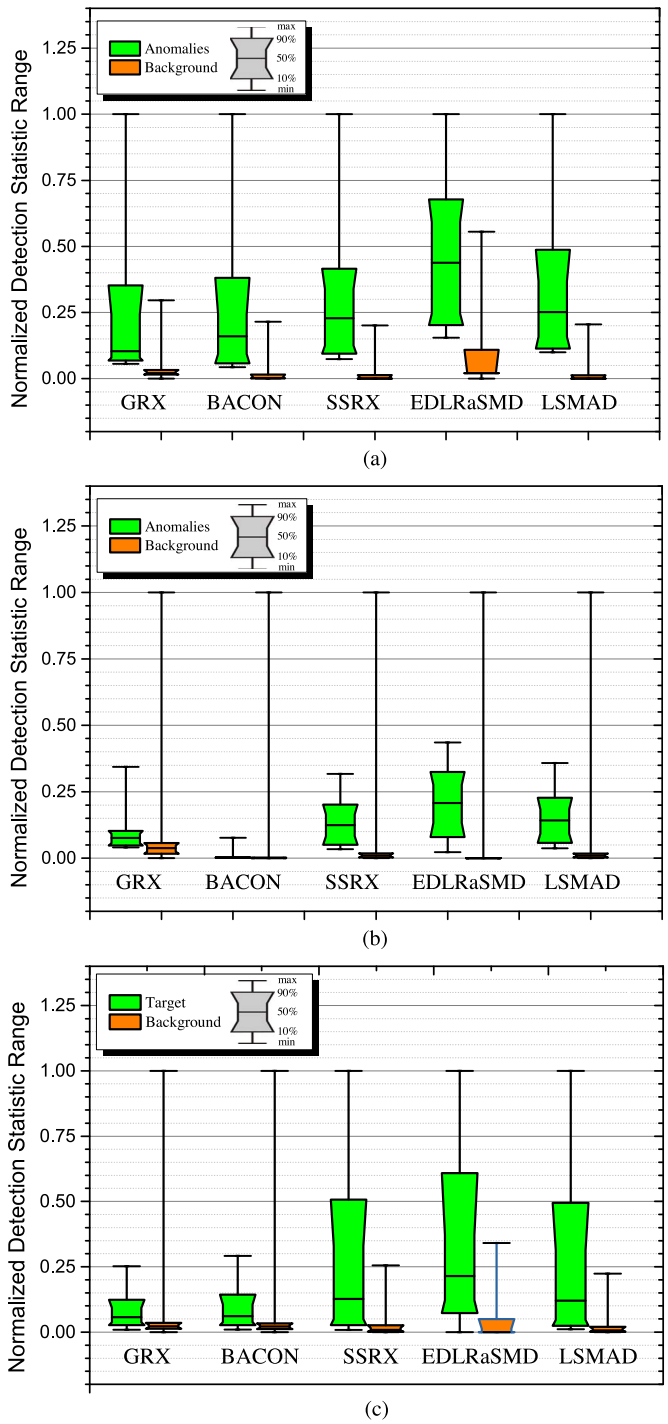

Fig. 10. Separability maps of the five detectors for the three data sets. (a) PaviaC. (b) AVIRIS. (c) Cri.

low-rank sparse-decomposition-based methods also draw the same conclusions [16], [35]–[38]. The sparse component in the LRaSMD model may contain some background energy; thus, not all the background materials are taken into consideration when determining the rank value of the low-rank component. This provides a possible explanation that a very low rank value is preferred. In addition, based on the analysis of [35], the rank of the background component matrix is highly correlated with the number of the classes; thus, another possible way to estimate rank value empirically is to determine it by the number of the main background categories of the HSIs.

In addition, the performance of LSMAD with respect to the cardinality parameter k of the sparse matrix was analyzed. The cardinality k of the sparse matrix was set between the relaxed

Authorized licensed use limited to: FUDAN UNIVERSITY. Downloaded on February 26,2022 at 02:06:20 UTC from IEEE Xplore. Restrictions apply.

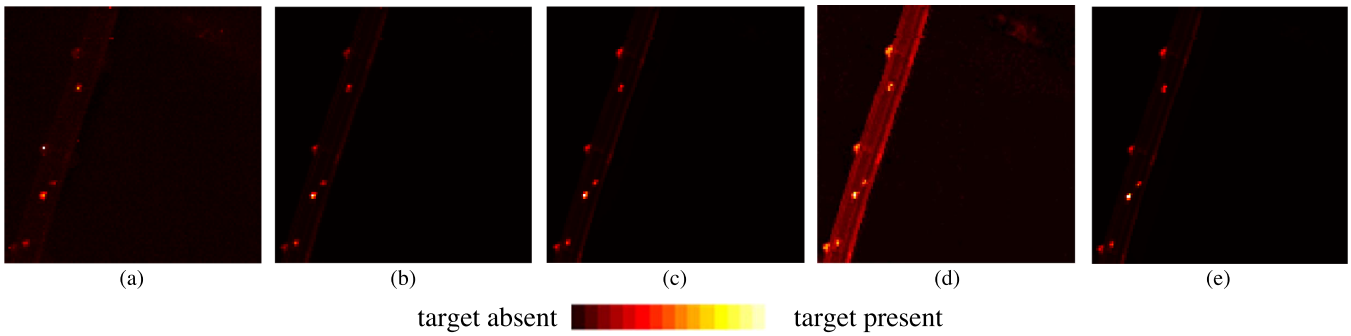

Fig. 11. Two-dimensional plots of the detection test statistic results for the PaviaC data set. (a) GRX. (b) BACON. (c) SSRX. (d) EDLRaSMD. (e) LSMAD.

RAI value and 1 for the three data sets. For convenience and accuracy, we set a small step size from the lower limit value to 0.1 and then set a larger step size from 0.1 to 1. The value of r was set between 1 and 10 for convenience. The experimental results are provided via AUCs.

From the results for LSMAD in Fig. 9, we can see that the AUC value remains almost the same as the value of k increases at each rank value. Based on the aforementioned results, we can make the following summary. LSMAD can achieve a good detection performance over a broad range of k values. The reason for this may be as follows. The cardinality parameter controls the sparse energy in the sparse matrix. Increasing the value of k from a small value therefore leads to more and more distinctive features of the anomalies being included in the sparse matrix. However, with the continued increase in k, some spectral features of the background pixels will be also included in the sparse matrix, which decreases the separability between anomalies and background. However, the few included anomaly pixels will have very little effect on the background statistics estimation for LSMAD.

To further investigate the ability of LSMAD to distinguish anomalies from the background, the separability between anomalies and background was evaluated and compared with the other detectors via separability maps, as shown in Fig. 10. After statistical calculation of the detection values of each pixel, boxes are drawn to enclose the main parts of the pixels, excluding the biggest 10% and the smallest 10%. There are anomaly and background columns for each detector. The lines at the top and bottom of each column are the extreme values, which are normalized to 0–1. The green boxes illustrate the distribution of the anomaly pixels' values, and the line in the middle of the box is the mean of the pixels. In a similar way, the orange boxes enclose the middle 80% of the main pixels of the background pixels. The position of the boxes reflects the tendency and compactness of the distribution of the pixels. In other words, the position reflects the separability of the anomalies and background.

For the PaviaC data set, as shown in Fig. 10(a), BACON and SSRX gradually and successively increase the gap between the anomaly box and the background box compared with that for GRX. The gaps between the two boxes for SSRX, EDLRaSMD, and LSMAD are very obvious, and the gap for LSMAD is slightly bigger. Compared with EDLRaSMD, LSMAD can effectively suppress the background information in this data set, particularly the middle 80% of the main background pixels. For the AVIRIS data set, as shown in Fig. 10(b), the detection becomes complicated as the gaps between the anomaly and background boxes for all the detectors are much smaller than those for the other data sets. The anomaly box is overlapped with the background box for GRX and BACON. The gap between the anomaly and background boxes for LSMAD is slightly bigger than that for SSRX. For the Cri data set, as shown in Fig. 10(c), the detection becomes complicated as there are hardly any gaps between the anomaly and background boxes for almost all the detectors. However, LSMAD can still effectively suppress the background information in this data set.

Based on the aforementioned results, we can see that LSMAD generally performs better than GRX and BACON, as the gaps between the anomaly and background boxes are clearly bigger than those for GRX and BACON with the PaviaC and AVIRIS data sets, and the performance in suppressing the background information is slightly better with the Cri data set. LSMAD also performs better than SSRX, as the gaps between the anomaly and background boxes are slightly bigger than those for SSRX with the PaviaC and AVIRIS data sets, and the performance in suppressing the background information is slightly better with the Cri data set. Furthermore, LSMAD generally outperforms EDLRaSMD, as the gap between the anomaly and background boxes is bigger than that for EDLRaSMD with the PaviaC data set, and the performance in suppressing the background information is also better than that for EDLRaSMD with the PaviaC and Cri data sets.

Finally, 2-D plots of the detection test statistic results of all the comparison algorithms with the three data sets are shown in Figs. 11–13. For the PaviaC data set, as shown in Fig. 11, we can see that the proposed LSMAD provides a distinguishable statistic map compared with EDLRaSMD, which shows high statistical values for the background bridge pixels. However, the differences between LSMAD and the other four detectors are subtle, and they are not easily differentiated. For the AVIRIS data set, as shown in Fig. 12, LSMAD presents a clearly distinguishable statistic map compared with all the other detectors. SSRX and EDLRaSMD also show high statistical values for the anomaly pixels, but compared with LSMAD, some tree or grass pixels, particularly in the bottom left corner in the image, also output high values, which would cause false alarms. For the Cri data set, as shown in Fig. 13, LSMAD presents a clearly distinguishable statistic map compared with GRX, BACON,

Authorized licensed use limited to: FUDAN UNIVERSITY. Downloaded on February 26,2022 at 02:06:20 UTC from IEEE Xplore. Restrictions apply.

(a) (b) (c) (d) (e)

Fig. 12. Two-dimensional plots of the detection test statistic results for the AVIRIS data set. (a) GRX. (b) BACON. (c) SSRX. (d) EDLRaSMD. (e) LSMAD.

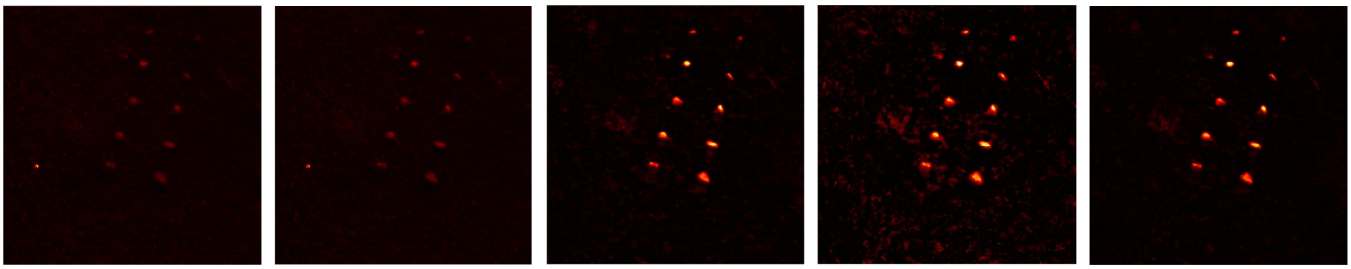

(a) (b) (c) (d) (e)

Fig. 13. Two-dimensional plots of the detection test statistic results for the Cri data set. (a) GRX. (b) BACON. (c) SSRX. (d) EDLRaSMD. (e) LSMAD.

and EDLRaSMD. However, the differences between LSMAD and SSRX are subtle when viewed with the naked eye. It can be seen that EDLRaSMD outputs high statistical values for the anomaly pixels, but many other pixels in the image also output high values, which would cause false alarms.

IV. Conclusion

In this paper, LSMAD has been proposed as a new perspective to employ LRaSMD for hyperspectral anomaly detection. Based on the consistency of the LRaSMD technique and the hyperspectral anomaly detection problem, this algorithm utilizes LRaSMD to obtain the low-rank background and the sparse component. The GoDec algorithm is then employed for the background and sparse components optimization problem. In order to avoid the unstable sparse component, the Mahalanobis distance is introduced by employing the estimated background component and imposing the low-rank background property for the inverse background covariance matrix estimation. This way, LSMAD is able to simultaneously alleviate the anomaly contamination, the inverse covariance matrix problem, and the LRaSMD parameter instability issue.

Experiments in hyperspectral detection with four data sets confirmed the superior performance of the proposed LSMAD algorithm. LSMAD presents a superior detection performance and separability ability when compared with the other state-of-the-art detectors. In general, with the HySime algorithm, the performances of LSMAD, EDLRaSMD, and SSRX, respectively, are decreased compared with that with the empirically determined rank values. Although the existed algorithms, such as the HySime algorithm, can provide a rank candidate without other supplementary information, they may not always provide the satisfactory detection performance. However, this empirically parameter selection method represents a limitation as regards operational applicability of the proposed approach in reality application, which will be the focus of our future work.

Acknowledgment

The authors would like to thank the handling editor and anonymous reviewers for their careful reading and helpful remarks.

References

[1] G. Shaw and D. Manolakis, "Signal processing for hyperspectral image exploitation," *IEEE Signal Process. Mag.*, vol. 19, no. 1, pp. 12–16, Jan. 2002.

[2] D. Landgrebe, "Hyperspectral image data analysis," *IEEE Signal Process. Mag.*, vol. 19, no. 1, pp. 17–28, Jan. 2002.

[3] M. Borengasser, W. S. Hungate, and R. Watkins, *Hyperspectral Remote Sensing—Principles and Applications*. Boca Raton, FL, USA: CRC Press, 2008.

[4] R. Zhao, B. Du, and L. Zhang, "A robust nonlinear hyperspectral anomaly detection approach," *IEEE J. Sel. Topics Appl. Earth Observ. Remote Sens.*, vol. 7, no. 4, pp. 1227–1234, Apr. 2014.

[5] B. Du and L. Zhang, "Random-selection-based anomaly detector for hyperspectral imagery," *IEEE Trans. Geosci. Remote Sens.*, vol. 49, no. 5, pp. 1578–1589, May 2011.

[6] C.-I. Chang, "Target signature-constrained mixed pixel classification for hyperspectral imagery," *IEEE Trans. Geosci. Remote Sens.*, vol. 40, no. 5, pp. 1065–1081, May 2002.

[7] I. C. Chein and C. Shao-Shan, "Anomaly detection and classification for hyperspectral imagery," *IEEE Trans. Geosci. Remote Sens.*, vol. 40, no. 6, pp. 1314–1325, Jun. 2002.

[8] D. Manolakis, D. Marden, and G. A. Shaw, "Hyperspectral image processing for automatic target detection applications," *J. Lincoln Lab.*, vol. 14, no. 1, pp. 79–116, 2003.

[9] J. E. Fowler and Q. Du, "Anomaly detection and reconstruction from random projections," *IEEE Trans. Image Process.*, vol. 21, no. 1, pp. 184–195, Jan. 2012.

[10] S. Matteoli, M. Diani, and G. Corsini, "A tutorial overview of anomaly detection in hyperspectral images," *IEEE Aerosp. Electron. Syst. Mag.*, vol. 25, no. 7, pp. 5–28, Jul. 2010.

Authorized licensed use limited to: FUDAN UNIVERSITY. Downloaded on February 26,2022 at 02:06:20 UTC from IEEE Xplore. Restrictions apply.

[11] D. W. J. Stein *et al.*, "Anomaly detection from hyperspectral imagery," *IEEE Signal Process. Mag.*, vol. 19, no. 1, pp. 58–69, Jan. 2002.
[12] I. S. Reed and X. Yu, "Adaptive multiple-band CFAR detection of an optical pattern with unknown spectral distribution," *IEEE Trans. Acoust. Speech Signal Process.*, vol. 38, no. 10, pp. 1760–1770, Oct. 1990.
[13] A. P. Schaum, "Joint subspace detection of hyperspectral targets," in *Proc. IEEE Aerosp. Conf.*, 2004, pp. 1818–1824.
[14] S. Matteoli, M. Diani, and G. Corsini, "Impact of signal contamination on the adaptive detection performance of local hyperspectral anomalies," *IEEE Trans. Geosci. Remote Sens.*, vol. 52, no. 4, pp. 1948–1968, Apr. 2014.
[15] M. D. Farrell and R. M. Mersereau, "On the impact of covariance contamination for adaptive detection in hyperspectral imaging," *IEEE Signal Process. Lett.*, vol. 1, no. 9, pp. 649–652, Sep. 2005.
[16] N. Billor, S. Hadia, and P. F. Velleman, "BACON: Blocked adaptive computationally efficient outlier nominators," *Comput. Statist. Data Anal.*, vol. 34, no. 3, pp. 279–298, Sep. 2000.
[17] T. E. Smetek and K. W. Bauer, "Finding hyperspectral anomalies using multivariate outlier detection," in *Proc. IEEE Aerosp. Conf.*, 2007, pp. 1–24.
[18] S. Matteoli, M. Diani, and G. Corsini, "Hyperspectral anomaly detection with Kurtosis-driven local covariance matrix corruption mitigation," *IEEE Geosci. Remote Sens. Lett.*, vol. 8, no. 3, pp. 532–536, May 2011.
[19] A. Banerjee, P. Burlina, and C. Diehl, "A support vector method for anomaly detection in hyperspectral imagery," *IEEE Trans. Geosci. Remote Sens.*, vol. 44, no. 8, pp. 2282–2291, Aug. 2006.
[20] S. Khazai, S. Homayouni, A. Safari, and B. Mojaradi, "Anomaly detection in hyperspectral images based on an adaptive support vector method," *IEEE Geosci. Remote Sens. Lett.*, vol. 8, no. 4, pp. 646–650, Jul. 2011.
[21] E. J. Candès, X. Li, Y. Ma, and J. Wright, "Robust principal component analysis?" *J. ACM*, vol. 58, no. 3, pp. 1–37, May 2011.
[22] A. Sumarsono and Q. Du, "Robust principal component analysis for hyperspectral anomaly detection," in *Proc. IEEE IGARSS*, 2014, pp. 1–4.
[23] L. Xiong, X. Chen, and J. Schneider, "Direct robust matrix factorization for anomaly detection," in *Proc. IEEE ICDM*, 2011, pp. 1–10.
[24] X. Cui, Y. Tian, L. Weng, and Y. Yang, "Anomaly detection in hyperspectral imagery based on low-rank and sparse decomposition," in *Proc. 5th ICGIP*, 2013, vol. 9069, 1–73.
[25] W. Sun, C. Liu, J. Li, Y. M. Lai, and W. Li, "Low-rank and sparse matrix decomposition-based anomaly detection for hyperspectral imagery," *J. Appl. Remote Sens.*, vol. 8, no. 1, pp. 1–18, May 2014.
[26] Y. Chen, N. M. Nasrabadi, and T. D. Tran, "Sparse representation for target detection in hyperspectral imagery," *IEEE J. Sel. Topics Signal Process.*, vol. 5, no. 3, pp. 629–640, Jun. 2011.
[27] M. Golbabaee and P. Vandergheynst, "Hyperspectral image compressed sensing via low-rank and joint-sparse matrix recovery," in *Proc. IEEE ICASSP*, 2012, pp. 2741–2744.
[28] K. Rong, S. Wang, X. Zhang, and B. Hou, "Low-rank and sparse matrix decomposition-based pan sharpening," in *Proc. IEEE IGARSS*, 2012, pp. 2276–2279.
[29] Y. Xue, X. Guo, and X. Cao, "Motion saliency detection using low-rank and sparse decomposition," in *Proc. IEEE ICASSP*, 2012, pp. 1485–1488.
[30] Y. Zhang, B. Du, and L. Zhang, "Regularization framework for target detection in hyperspectral imagery," *IEEE Geosci. Remote Sens. Lett.*, vol. 11, no. 1, pp. 313–317, Jan. 2014.
[31] Z. Zhou, X. Li, J. Wright, E. J. Candès, and Y. Ma. "Stable principal component pursuit," in *Proc. IEEE ISIT*, 2010, pp. 1518–1522.
[32] T. Zhou, D. Tao, and X. Wu, "Manifold elastic net: A unified framework for sparse dimension reduction," *Data Mining Knowl. Discovery*, vol. 22, no. 3, pp. 340–371, May 2011.
[33] N. Halko, P. G. Martinsson, and J. A. Tropp, "Finding structure with randomness: Stochastic algorithms for construction approximate matrix decompositions," *SIAM Rev.*, vol. 53, no. 2, pp. 217–288, May 2009.
[34] T. Zhou and D. Tao, "Godec: Randomized low-rank & sparse matrix decomposition in noisy case," in *Proc. 28th ICML*, 2011, pp. 33–40.
[35] T. Zhou and D. Tao, "Bilateral random projection," in *Proc. IEEE ISIT*, 2012, pp. 1286–1290.
[36] H. Viljoen and J. H. Venter, "Identifying multivariate discordant observation: A computer-intensive approach," *Comput. Statist. Data Anal.*, vol. 40, no. 1, pp. 159–172, Jul. 2002.
[37] L. H. Chiang, R. J. Pell, and M. B. Seasholtz, "Exploring process data with the use of robust outlier detection algorithms," *J. Process Control*, vol. 13, no. 5, pp. 437–449, Aug. 2003.
[38] C. Becker and U. Gather, "The masking breakdown point of multivariate outlier identification rules," *J. Amer. Stat. Assoc.*, vol. 94, no. 447, pp. 947–955, Sep. 1999.
[39] Y. Gu, C. Wang, S. Wang, and Y. Zhang, "Kernel-based regularized-angle spectral matching for target detection in hyperspectral imagery," *Pattern Recognit. Lett.*, vol. 32, no. 2, pp. 114–119, Jan. 2011.
[40] L. Zhang, L. Zhang, D. Tao, and X. Huang, "Sparse transfer manifold embedding for hyperspectral target detection," *IEEE Trans. Geosci. Remote Sens.*, vol. 52. no. 2, pp. 1030–1043, Feb. 2014.
[41] L. Zhang, B. Du, and Y. Zhong, "Hybrid detectors based on selective endmembers," *IEEE Trans. Geosci. Remote Sens.*, vol. 48, no. 6, pp. 2633–2646, Jun. 2010.
[42] W. Li and Q. Du, "Collaborative representation for hyperspectral anomaly detection," *IEEE Trans. Geosci. Remote Sens.*, vol. 53, no. 3, pp. 1463–1474, Mar. 2015.
[43] L. Ma, M. M. Crawford, and J. Tian, "Anomaly detection for hyperspectral images based on robust locally linear embedding," *J. Infrared*, vol. 31, no. 6, pp. 753–762, Jun. 2010.
[44] A. Sumarsono and Q. Du, "Low-rank subspace representation for estimating the number of signal subspaces in hyperspectral imagery," *IEEE Trans. Geosci. Remote Sens.*, vol. 53, no. 11, pp. 6286–6292, Nov. 2015.
[45] X. Yuan and J. Yang, "Sparse and low-rank matrix decomposition via alternating direction methods," *Pacific J. Optim.*, vol. 9, no. 1, pp. 1–11, 2009.
[46] H. Zhang, W. He, L. Zhang, H. Shen, and Q. Yuan, "Hyperspectral image restoration using low-rank matrix recovery," *IEEE Trans. Geosci. Remote Sens.*, vol. 52, no. 8, pp. 4729–4743, Aug. 2014.
[47] J. M. Bioucas-Dias and J. M. P. Nascimento, "Hyperspectral subspace identification," *IEEE Trans. Geosci. Remote Sens.*, vol. 46, no. 8, pp. 2435–2445, Aug. 2008.

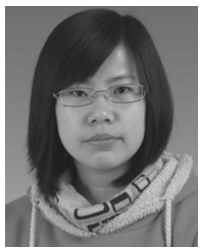

Yuxiang Zhang (S'13) received the B.S. degree in sciences and techniques of remote sensing from Wuhan University, Wuhan, China, in 2011. She is currently working toward the Ph.D. degree in sciences and techniques of remote sensing at Wuhan University.

Her research interests include hyperspectral image processing, target detection, sparse representation, and signal processing.

Bo Du (M'10–SM'15) received the B.S. degree in engineering and the Ph.D. degree in photogrammetry and remote sensing from Wuhan University, Wuhan, China, in 2005 and 2010, respectively.

He is currently an Associate Professor with the School of Computer, Wuhan University. He has over 20 research papers published in journals such as the IEEE TRANSACTIONS ON IMAGE PROCESSING (TIP), the IEEE JOURNAL OF SELECTED TOPICS IN EARTH OBSERVATIONS AND APPLIED REMOTE SENSING (JSTARS), and the IEEE GEOSCIENCE AND REMOTE SENSING LETTERS (GRSL), among others. His major research interests include pattern recognition, hyperspectral image processing, and signal processing.

Prof. Du serves as a Reviewer of over 20 Science Citation Index magazines, including IEEE TRANSACTIONS ON GEOSCIENCE AND REMOTE SENSING, TIP, JSTARS, and GRSL.

Authorized licensed use limited to: FUDAN UNIVERSITY. Downloaded on February 26,2022 at 02:06:20 UTC from IEEE Xplore. Restrictions apply.

Liangpei Zhang (M'06–SM'08) received the B.S. degree in physics from Hunan Normal University, Changsha, China, in 1982, the M.S. degree in optics from the Xi'an Institute of Optics and Precision Mechanics, Chinese Academy of Sciences, Xi'an, China, in 1988, and the Ph.D. degree in photogrammetry and remote sensing from Wuhan University, Wuhan, China, in 1998.

He is currently the Head of the Remote Sensing Division, State Key Laboratory of Information Engineering in Surveying, Mapping and Remote Sensing, Wuhan University. He is also a "Chang-Jiang Scholar" Chair Professor appointed by the Ministry of Education of China. He is currently a Principal Scientist for the China State Key Basic Research Project (2011–2016) appointed by the Ministry of National Science and Technology of China to lead the remote sensing program in China. He has over 450 research papers and five books. He is the holder of 15 patents. His research interests include hyperspectral remote sensing, high-resolution remote sensing, image processing, and artificial intelligence.

Dr. Zhang is a Fellow of The Institution of Engineering and Technology. He is the Founding Chair of the IEEE Geoscience and Remote Sensing Society (GRSS) Wuhan Chapter. He was the General Chair for the Fourth IEEE GRSS Workshop on Hyperspectral Image and Signal Processing: Evolution in Remote Sensing. He is an Executive Member (Board of Governors) of the China National Committee of International Geosphere-Biosphere Programme and an Executive Member of the China Society of Image and Graphics, etc. He regularly serves as a Cochair of the series SPIE Conferences on Multispectral Image Processing and Pattern Recognition, Conference on Asia Remote Sensing, and many other conferences. He edits several conference proceedings, issues, and geoinformatics symposiums. He is currently serving as an Associate Editor of the IEEE TRANSACTIONS ON GEOSCIENCE AND REMOTE SENSING. He also serves as an Associate Editor of the *International Journal of Ambient Computing and Intelligence*, the *International Journal of Image and Graphics*, the *International Journal of Digital Multimedia Broadcasting*, the *Journal of Geo-spatial Information Science*, and the *Journal of Remote Sensing* and a Guest Editor of the *Journal of Applied Remote Sensing* and the *Journal of Sensors*. He has been a Guest Editor of the IEEE JOURNAL OF SELECTED TOPICS IN EARTH OBSERVATIONS AND APPLIED REMOTE SENSING (JSTARS). He was a recipient of the 2010 Boeing Best Paper Award and the 2013 ERDAS Best Paper Award from the American Society of Photogrammetry and Remote Sensing. He was also a recipient of the best reviewer awards from IEEE GRSS for his service to IEEE JSTARS in 2012 and the IEEE Geoscience and Remote Sensing Letters in 2014. His research teams won the top three prizes of the IEEE Geoscience and Remote Sensing Society 2014 Data Fusion Contest, and his students have been selected as the winners or the finalists of the IEEE International Geoscience and Remote Sensing Symposium student paper contest in recent years.

Shugen Wang (M'03) received the B.S. degree in aerial photogrammetry from Wuhan College of Surveying and Mapping, Wuhan, China, in 1984, the M.S. degree in photogrammetry and remote sensing from Wuhan University of Surveying and Mapping Science and Technology, Wuhan, in 1994, and the Ph.D. degree in photogrammetry and remote sensing from Wuhan University, Wuhan, in 2003.

He is currently a Professor with the School of Remote Sensing and Information Engineering, Wuhan University. His major research interests include digital photogrammetry, high-spatial-resolution remote sensing image processing, and computer vision.

Authorized licensed use limited to: FUDAN UNIVERSITY. Downloaded on February 26,2022 at 02:06:20 UTC from IEEE Xplore. Restrictions apply.